Magnetic (hyper)thermia or photo-thermia? Progressive comparison of iron oxide and gold nanoparticles heating in water, in cells, and *in vivo*

Ana Espinosa*[1], Jelena Kolosnjaj-Tabi[1], Ali Abou-Hassan[2], Anouchka Plan Sangnier[1], Alberto Curcio[1], Amanda Silva[1], Riccardo Di Corato[1], Sophie Neveu[2], Teresa Pellegrino[3], Luis M Liz-Marzán[4,5], Claire Wilhelm*

1. Laboratoire Matière et Systèmes Complexes, UMR 7057, CNRS and University Paris Diderot, 75205 Paris cedex 13, France. ana.espinosa@univ-paris-diderot.fr, claire.wilhelm@univ-paris-diderot.fr

2. Sorbonne Université, CNRS, PHysico-chimie des Electrolytes et Nanosystèmes InterfaciauX, PHENIX, F-75005 Paris, France.

3. Istituto Italiano di Tecnologia, I-16163 Genoa, Italy

4. CIC biomaGUNE and Ciber-BBN, Paseo de Miramón 182, 20009 Donostia, San Sebastián, Spain

5. Ikerbasque, Basque Foundation for Science, 48013 Bilbao, Spain

ABSTRACT

Magnetic hyperthermia (MHT) and photothermal therapy (PTT) are the emergent state-of-the-art modalities for thermal treatment of cancer. While their mechanisms of action have distinct physical bases, the common feature between these two heat-generating techniques is the nanoparticle-mediated, remote onset of the therapy. Yet, are the two heating techniques interchangeable? Here, we compare MHT and PTT, applying the same methodologies, on multiple levels and distinct environments, for a set of nanomaterials differing in shape (spheres, cubes, stars, shells and rods) and in composition (iron oxides including maghemite, magnetite, and cobalt ferrite; and gold). In a first-tier test, we assessed the nanoparticles heating efficacy (–expressed in W/g) in an aqueous environment, at a given concentration of iron or gold. Secondly, we evaluated the heating efficiency within the cellular environment. Intracellular processing markedly impacted MHT, where the significant loss of heating performance is attributed to confinement of the nanoparticles within endosomes. Conversely, little if any of such confinement effects were detected in PTT. On the contrary, for plasmonic nanoparticles, endosomal sequestration can have a positive effect on light-induced heating. Finally, we selected iron oxide nanocubes and gold nanostars to evidence a dose-dependent heat generation in PTT, and to compare MHT and PTT *in vivo* within the heterogeneous intratumoral environment.

The gathered data clearly evidence two distinct therapeutic approaches, related to high dosage allowing MHT and low dosage associated with PTT (mediated by either plasmonic or magnetic nanoparticles). They also indicate that PTT mediated by magnetic nanoparticles has an efficacy that is unexpectedly comparable to that of plasmonic nanoparticles PTT, but only for suitable nanoparticles concentration. At low concentration, only plasmonic nanoparticles can deliver a therapeutic heating under PTT.

Keywords: Magnetic hyperthermia, Photothermal therapy, Magnetic nanoparticles, Plasmonic nanoparticles, Iron Oxide, Gold, Nanomedicine.

INTRODUCTION

The promising expectations of prospective nano-physical treatments in cancer therapies rely on the nanoparticles potential to exert a physical effect on target tissues (*e.g.* emit heat or deploy a mechanical force) after being excited by a remote source of energy (*e.g.* light,[1] magnetism,[2] radiofrequency electric field[3]). Nanoparticles allying the effects of specific inorganic components (made of a magnetic and/or a metallic part) with the action of molecular constituents (*i.e.* chemotherapy drugs, specific receptor ligands, antibodies, polymer coatings), could thus exert a highly localized action.[4] The latter could be triggered by a physical stimulus that would be set on with precise temporal and spatial control, which could minimize potential adverse reactions occurring in healthy tissue.

In nanoparticle-mediated thermal therapies, heat dissipation phenomena are produced by the fluctuations of magnetic moment in magnetic nanoparticles (magnetic hyperthermia, MHT)[5] or charge-density oscillations in metallic nanoparticles (photothermia, also called photothermal therapy, PTT).[6] In MHT, magnetic nanoparticles, considered as individual magnetic dipoles, orient their magnetic moments after exposure to an alternating magnetic field (AMF). The magnetic energy is dissipated through the relaxation of the nanoparticles moment to equilibrium, either through the rotation of the nanoparticle as a whole (Brown relaxation) or through the rotation of the magnetic moment within the nanoparticle core (Néel relaxation). The heat-generating potential of magnetic nanoparticles then depends on nanoparticles structure, size and magnetic anisotropy. In PTT, plasmonic nanoparticles absorb energy due to the interactions of light with conduction band electrons on the metallic nanoparticle surface and part of this energy is released as heat. When the illumination wavelength is in resonance with the surface plasmon frequency (localized surface plasmon resonance, or LSPR), absorption results in optimal heat dissipation. The LSPR frequency is defined by the nanoparticles size, shape and local environment.

This ability of magnetic and metallic (plasmonic) nanoparticles to be remotely activated *via* physical stimuli (alternating magnetic field or light, respectively) and generate heat, might be used as a tool to damage malignant cells. Magnetic hyperthermia (MHT[5, 7, 8]) and photothermia (PTT[9, 10]) thus recently made a breakthrough either as standalone therapies or as adjuvant treatments of cancer. As in conventional hyperthermia treatments (such as the ones employing thermal

chambers, ultrasound, microwave or radiofrequency), the aim of MHT and PTT is to rise the tissue temperature to the range of 40 to 45 °C. Yet, unlike in conventional treatments, where the heat is focalized on larger zones of the body, the ambition of MHT and PTT is to locally target cancer cells and selectively damage them without harming the surrounding healthy tissue.

Multiple factors make thermal treatments particularly appealing in oncology:

(i) Effect of hyperthermia on the cellular level: Within the cell, nuclear proteins show the greatest sensitivity to heat, which affects inhibition of DNA repair and replication, as well as RNA and protein synthesis.[11] Hyperthermia also results in the disaggregation of microtubules and microfilaments. Cells exhibiting the highest heat sensitivity are in the S- and M- phase, resulting in chromosomal damage, and inefficient mitosis, respectively.

(ii) The tumors and the body behave differently against heat-induced damage: At tissue temperature levels up to 45 °C, exposure times of 30 to 60 minutes and heating rates up to 0.7 °C/min, the vasculature of healthy tissues readily increases their blood flow (or perfusion), which dissipates heat and prevents excessive heating of tissues.[12] The tumor vasculature, on the other hand, is hyper-permeable, tortuous, disorganized, and overflows with blind ends and abnormal bulges,[13] making tumors much less efficient in heat dissipation. Thus, at the same thermal dose, the healthy tissue surrounding the tumor can remain at a lower temperature than the tumor itself (*e.g*. the temperature of the tumor might rise up to 50 °C while the periphery stays at 45 °C, thus hyperthermia does not harm adjacent tissues/organs,[14] while blood supply in tumors collapses during or after heating). However, a prolonged exposure to higher thermal doses induces the inhibition of the blood perfusion within the tumor and the increased rigidity of red blood cells, which result in vasodilatation, blood stasis, endothelial swelling, disintegration of endothelial lining, and plasma leakage or hemorrhage, with red blood cell and platelet aggregation leading to coagulative necrosis. The altered blood flow also affects oxygen and nutrient delivery within the tumor and prevents the removal of lactic acid, leading to severe tissue acidosis within the tumors.

(iii) Effects on the extracellular matrix: Apart from acting on tumor cells and vasculature, nanoparticle-induced hyperthermia affects the extracellular matrix.[15-17] Its

essential constituents, the collagen fibers, slacken during hyperthermia, which allows a better spreading/penetration of chemotherapeutics.[16]

(iv) Imperceptible hyperthermia: In contrast to the overt hyperthermia of tumors, recent research shows that heating nanoparticles may also lead to cell death without a perceptible macroscopic temperature increase.[18-20] The subcellular temperature increase, focally localized within lysosomes, might induce cell death through lysosomal death pathways, and thus might probably be applicable to apoptosis-resistant cancer cells.[20]

Due to all these therapeutic benefits of thermal tumor treatments, and more specially, to the potent local nanothermic action, magnetic nanoparticles-mediated hyperthermia and nanoparticles-mediated photothermal therapy have been extensively studied in pre-clinical settings, and have recently also translated into clinical evaluations (clinical trials NCT02033447 (prostate), DRKS00005476 (glioblastoma) for MHT; NCT00848042 (head and neck tumors), NCT01679470 (primary and metastatic lung tumors) for PTT).

Until very recently, these thermal nanotherapies, MHT and PTT, have been studied and developed separately, resulting in two independent fields of thermal treatment. They have only recently begun to intersect due to the recent discovery and use of photothermal properties of iron oxide nanostructures[21, 22] or to the use of magneto-photothermal hybrids,[23] which combine both heating features in one-single object. These approaches of magneto-photo-thermia have brought improved therapeutic results to thermal nanotherapies, overcoming the relative advantages and disadvantages of both modalities, such as the low magnetic heating efficiency in cells or their limited sphere of action concerning deep-seated or superficial tumors.

Nevertheless, a toolbox is still needed to select the best nano-heater, leading to the most adequate heating delivery, for every thermal treatment. To fill this gap, we offer here a comprehensive comparison between MHT and PTT. This survey was conducted in environments of increasing biological complexity: in the aqueous environment, inside cells, and finally, within tumors. In addition, we thoroughly assessed the effect of the dose. The comparison was made in relation to the composition of the material (gold, iron oxide or cobalt ferrite), its shape (spheres, cubes, stars, rods and shells), and heating modality (PTT or MHT).

RESULTS AND DISCUSSION

1. A selection of state-of-the-art magnetic and plasmonic nanoparticles: the comparison of their heating capacities within the same experimental settings

The state-of-the-art nanoparticles intended for thermal therapies include magnetic (mainly iron oxide) or plasmonic (principally gold) nanoparticles, either of which exhibit a heating efficacy that correlates with their nanoscale-design.

The features that characterize the heating performance of magnetic nanoparticles include size, shape, anisotropy, magnetic exchange coupling, and saturation magnetization. The heating performance of plasmonic nanoparticles also depends on the size, but the essential parameter governing their suitability for thermal therapies *in vivo*, is particle shape. A specific shape will enable the particles to absorb (exhibit plasmon resonance) in the near-infrared wavelengths (generally between 650 to 1000 nm),[24, 25] where the optical absorption of tissues[25] is minimal and the treatment therefore attains the maximum penetration depth. Treatment depths of 4 to 6 mm have been reported for intratumorally injected gold nanoshells,[24] but the treatment range might differ in other tissues, which exhibit a different pigmentation and different perfusion. In addition, the treatment depth may be increased at lower particle concentrations, higher laser power and/or extended irradiation times.

In order to compare MHT and PTT, a set of eight state-of-the-art nanoparticles were selected and produced (Fig. 1). Magnetic particles (Fig. 1A) include rock-like 9-11 nm maghemite nanoparticles (IONPs - γFe_2O_3) and cobalt ferrite nanoparticles (CFNPs - $CoFe_2O_4$), both obtained by co-precipitation; 20-nm magnetite nanocubes (IONCs - Fe_3O_4) made by thermal decomposition; and 25-nm maghemite nanoflowers (IONFs - γFe_2O_3) prepared by means of the polyol process.

All of these selected magnetic nanoparticles display high saturation magnetization values, in the 70-80 emu/g range (Fig. 1C). Figure 1D also summarizes their absorbance, emphasizing privileged near infrared light absorption of IONCs and CFNPs. The optical absorbance as a function of iron content is shown in Figure S1 ([Fe] = 0.75-25 mM for all magnetic materials).

For what concerns plasmonic nanoparticles (Figure 1B), we selected two representative samples of gold nanostars (with overall sizes of 25 and 85 nm), which display LSPR bands red-shifting in the near-infrared (NIR) for increasing particle size,

centered at about 650 and 800, respectively (Fig. 1E). In addition to nanostars, nanorods and nanoshells were also selected, both of them exhibiting plasmon maxima at about 800 nm (Fig. 1E). Variation of the absorbance spectra with gold concentration can be seen in Figure S2. Table S1 also provides the total molar extinction coefficient ε (expressed in $M^{-1}.cm^{-1}$, either as moles of Fe or Au, or moles of nanoparticles) of magnetic and plasmonic nanoparticles calculated from the Beer-Lambert law at 680 and 808 nm. Gold nanoparticles have large extinction coefficients, in the $10^9 – 10^{10}$ M^{-1} cm^{-1} range, making them strong light absorbers close to their LSPR. Similar results were obtained in the literature for gold nanostars,[26] nanoshells[24] and nanorods.[27] These values are 4-5 orders of magnitude higher than those of magnetic nanoparticles (ε ~10^5-10^7) in the NIR range. Among the magnetic nanoparticles, IONC possess the highest molar extinction coefficient of $5x10^7$ M^{-1} cm^{-1} at 808 nm.

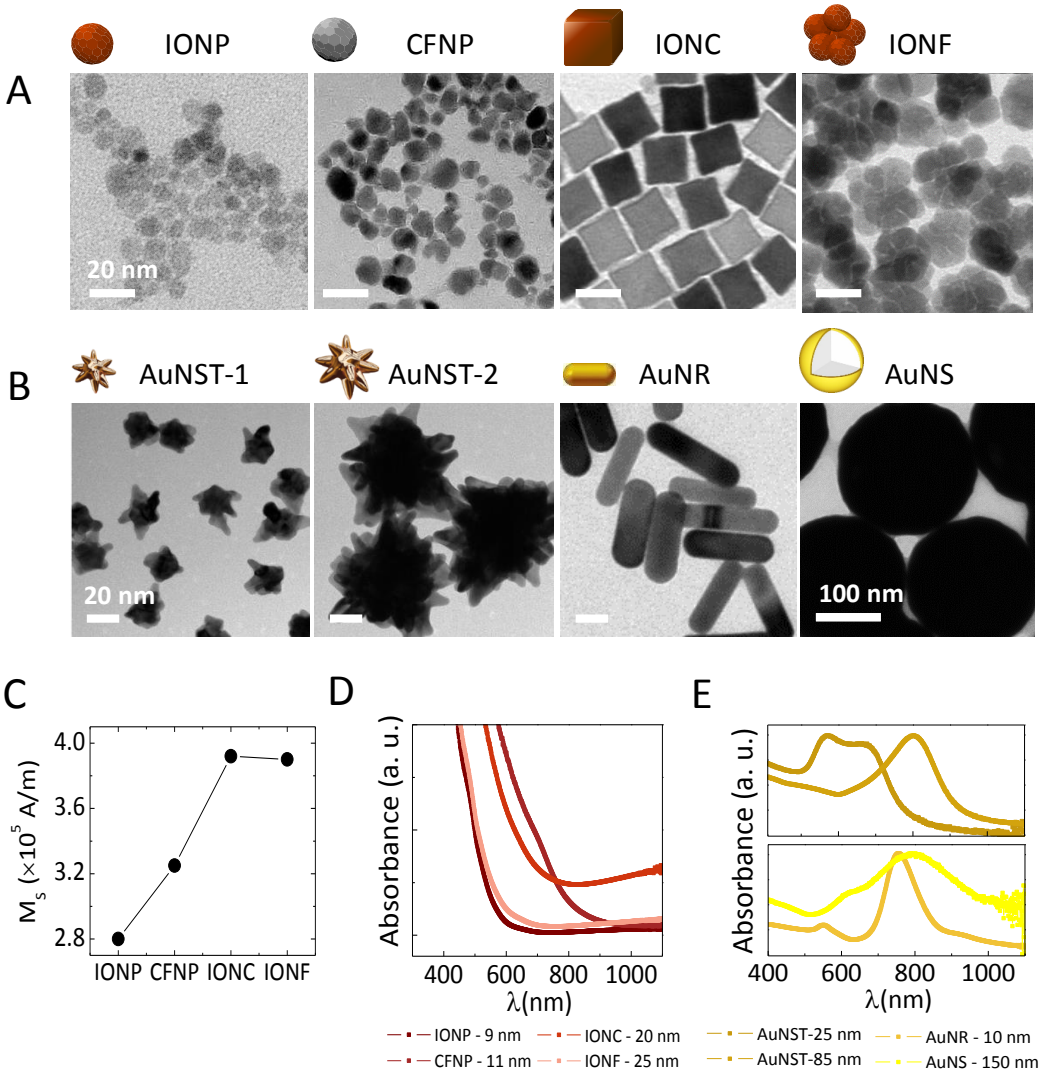

Fig. 1. Magnetic and metallic nanomaterials for thermal therapy. (**A)** Transmission electron microscopy (TEM) images of magnetic nanomaterials: iron oxide nanoparticles (IONP, 9 nm), cobalt ferrite nanoparticles (CFNP, 11 nm), iron oxide nanocubes (IONC, 20 nm) and iron oxide nanoflowers (IONF, 25 nm). (**B**) TEM micrographs of metallic nanomaterials: gold nanostars (AuNST, 25 and 85 nm), gold nanorods (AuNR, 10×40 nm) (20 nm scale bar) and gold nanoshells (AuNS, 150 nm). (**C**) Saturation magnetization at 300 K for all magnetic nanomaterials. Normalized UV-Vis-NIR spectra of (**D**) magnetic nanomaterials and (**E**) gold nanomaterials.

Fig. 2 summarizes the heating characteristics of all selected nanoparticle groups, measured under equal experimental conditions (identical volumes, tube types, thermalization, and same MHT and PTT conditions, alternating magnetic field and laser exposure), in water. The measurements were obtained at [Fe] = 25 mM (1.4 g_{Fe}/L) for all iron oxide nanoparticles, and at [Au] = 0.75 mM (0.15 g_{Au}/L) for gold nanoparticles, which are both typical concentrations used when testing the thermal potential of nanomaterials in aqueous dispersion. For gold nanoparticles, heating was measured under excitation conditions that correspond to the wavelength of plasmonic resonance for the given nanoparticles group (808 nm for gold nanorods, nanoshells and 85-nm nanostars, and 680 nm for the 25-nm nanostars). Figs. 2A and 2B show typical infrared images of the heating for all nanoparticles, and Figs. 2C and 2D show typical heating curves. The average temperature elevations after one-minute heating are shown for all conditions on Figs 2E and 2F.

Here it is worth to focus briefly on the applied experimental settings. MHT was performed at either 18 mT and 470 kHz (which is closer to the clinical limit, with H x f = 6.7×10^9 $Am^{-1}s^{-1}$)[5] or 24 mT and 900 kHz, which increases the thermal capacity of the particles, but is clinically less relevant. On the other hand, PTT was performed in the near infrared first biological transparency window, at 680 or 808 nm, and for two laser power densities (0.3 or 1 W/cm^2), considered in the range of tolerable laser powers,[28, 29] yet 0.3 W/cm^2 is more generally considered to be the clinical limit.[30]

Let us first note that (i) magnetic nanoparticles yield similar heat generation regardless of the type of magnetic or photonic activation; and (ii) plasmonic nanoparticles exhibit a comparable photo-activated heat generation, but for a molar concentration that is 30 times lower. The internal comparison between magnetic-nanoparticles mediated MHT and PTT (Fig. 2E) indicates that PTT, with the laser power density of 1 W/cm^2, leads to higher temperatures for IONCs and CFNPs, and to comparable temperatures at 0.3 W/cm^2. Conversely, IONFs, which display a high magnetic heating response, exhibit a

small photothermal efficiency. This is due to the low absorption of these particles in the NIR region (see Fig. S1), representative feature of maghemite-based nanoparticles (γFe_2O_3, as IONPs). In contrast, magnetite (Fe_3O_4) or cobalt ferrite ($CoFe_2O_4$) crystals exhibit higher absorbance in the NIR, due to charge transfer transitions between Fe^{2+} and Fe^{3+} ions in magnetite and magneto-optical transitions of Co^{2+} ions located in tetrahedral and octahedral coordination in the cobalt ferrite.[31-33]

While the temperature increase may depend on the experimental conditions (though it remains comparable among materials within the same environments), the concentration-renormalized slope of the temperature curve provides an absolute value representing the material's heating capacity (also known as the specific absorption rate, SAR) (Figs. 2G and H). The SAR, defined as the power absorbed per mass of material, is expressed in watt per gram (W/g). In the present study we determined the SAR per gram of iron pertaining to magnetic nanoparticles, or the SAR per gram of gold, contained in plasmonic nanoparticles. Considering magnetic nanoparticles, they reach a maximum of 400 W/g_{Fe} (for IONC and CFNP) in both MHT and PTT modalities for "safe" parameters exposure (18 mT and 470 kHz or 0.3 W/cm^2). For MHT, when the magnetic field and frequency are increased (up to clinically irrelevant ranges), the SAR may approach values of 1 kW/g_{Fe}. This value is what the literature generally considers as the upper limit of nanoparticles used in MHT,[5] emphasizing again that such SAR values are reported at clinically unacceptable magnetic field strengths/frequencies. In contrast, in the case of PTT, magnetic nanoparticles (IONP and CFNP) can reach 1 kW/g_{Fe} at more acceptable laser power densities of 1 W/cm^2. For plasmonic nanoparticles, the SARs (Fig. 2H) reach impressive values of 3 kW/g_{Au} or 10 kW/g_{Au}, at laser power densities of 0.3 W/cm^2 or 1 W/cm^2, respectively.

As a conclusion of this first-tier testing in aqueous medium, we ascertained the following. Firstly, plasmonic nanoparticles-mediated PTT has a higher thermal yield than magnetic nanoparticles-mediated MHT, as plasmonic nanoparticles resulted about 20 times more efficient, when the thermal efficacy was expressed in watts per gram of material (iron or gold). This is consistent with their much higher total molar extinction coefficient reflecting a higher absorption part (even though scattering effects cannot be neglected for large gold nanoparticles[6]). And secondly, irrespective of the fact that magnetic nanoparticles were used thus far mostly for MHT, we here confirm and substantiate more recent approaches that suggest their use as agents intended

for PTT,[21, 34-37] by showing that PTT values obtained at 1 W/cm² can be higher than the MHT-mediated ones.

From now on, in order to distinguish heat generation after either laser exposure of plasmonic nanoparticles, or laser exposure of magnetic nanoparticles, we will refer to "plasmonic PTT" or "magnetic PTT".

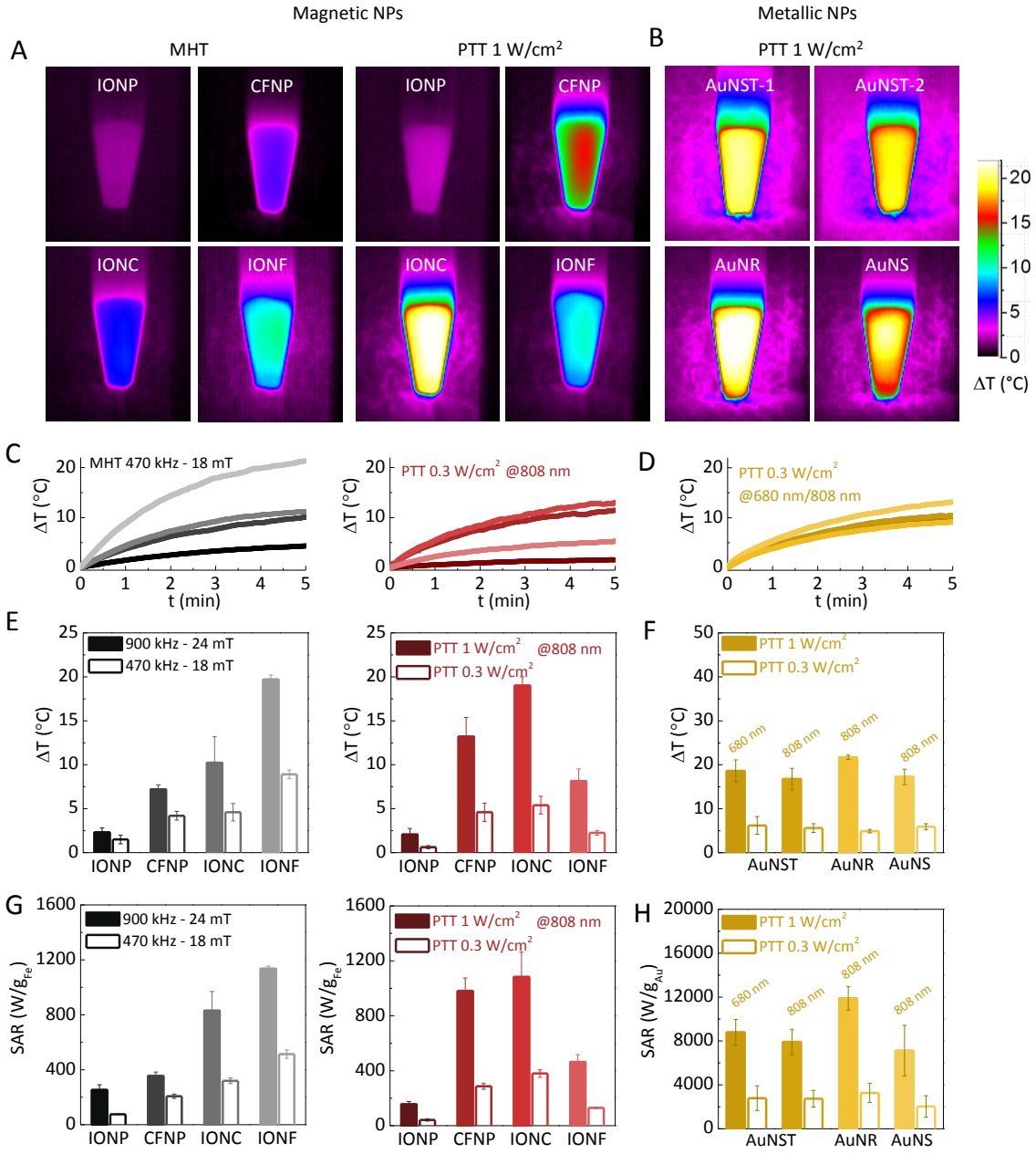

Fig. 2. Heating properties of selected nanomaterials in aqueous dispersion. **A.** Infrared thermal images of magnetic nanomaterials (IONP - 9 nm, CFNP -11 nm, IONC -20 nm and IONF - 25 nm) after 1 min of MHT at 470 kHz and 18 mT (MHT) and laser irradiation at 808 nm and 1 W/cm² (PTT). **B**. Infrared thermal images of selected metallic nanomaterials (AuNST-25 nm, and -85 nm, AuNR -10 nm and AuNS – 150 nm) after 1 min of laser irradiation at 680 or 808 nm (depending on LSPR) and 1 W/cm² (PTT). **C.** Typical temperature elevation curves of magnetic nanomaterials upon MHT

and PTT at low laser power conditions (0.3 W/cm²). **D**. Typical temperature elevations of metallic nanomaterials upon PTT at 0.3 W/cm². **E**. Average temperature increments for magnetic nanomaterials, subjected to alternating magnetic fields (MHT, at 900 kHz -24 mT and 470 kHz -18 mT) and to 808 nm-laser irradiation (PTT, 0.3 and 1 W/cm^2) at the same iron concentration [Fe] = 25 mM (1.4 g/L). **F**. Temperature increments for gold nanomaterials (PTT, 0.3 W/cm² and 1 W/cm^2, at 680 or 808 nm) at the same gold concentration [Au] = 0.75 mM (0.15 g/L). **G**, **H**. Heating capacities - SAR (W/g_{Fe} and W/g_{Au}) - of all nanomaterials.

2. The significance of concentration: a frequently disregarded parameter

The measurements obtained in the aforementioned first-tier testing were made at a specific concentration, as it is often the case in most reported studies. Nevertheless, how does the heating vary as a function of particle concentration? Is the SAR an independent and absolute parameter, which is completely unrelated to the concentration? It is the case for MHT, with rare exceptions at very high concentrations, where dipolar magnetic interparticle interactions may slightly impact the SAR. In PTT, on the other hand, we could expect that concentration does have an impact when the light absorption increases with concentration according to the Beer-Lambert law.

Indeed, as described in detail elsewhere,[38, 39] during the initial phase of heating (where heat dissipation can be neglected), the light-to-heat energy transfer can be written as $I_0.S.(1\text{-}10^{-A}).\eta=m_{sample}.C.dT/dt$, where I_0 (W) is the incident laser power, S (cm^2) is the illuminated area, A is the absorbance of the sample at the irradiation wavelength, η is the photothermal conversion efficiency from irradiation laser energy to thermal energy, m_{sample} the sample mass (here the mass of water), C the specific heat capacity (C_{water}= 4.18 J.g^{-1}.K^{-1}), and dT/dt the initial slope of the temperature increase. All samples tested here follow the Beer-Lambert law $A=\varepsilon.c.L$, with ε (M^{-1}cm^{-1}) the molar extinction coefficient (provided in Table S1), c the concentration of absorbing nanoparticles, and L the path length. Consequently, at high concentration, 10^{-A} becomes negligible, and the initial heating dT/dt remains almost constant with increasing concentrations. Note also that the SAR is expressed as ($m_{sample}.C/m_{Fe\ or\ Au}$).dT/dt (see the Methods section), and can thus be theoretically written as

$$SAR_{theor} = \frac{1}{m_{Fe\ or\ Au}}.[I_0.S.(1\text{-}10^{-A}).\eta] \qquad (1)$$

Fig. 3 compares the heating efficiency of magnetic and gold nanoparticles, with increasing mass concentrations of 0.05, 0.5 and 5 g/L. Concentrations are expressed in terms of grams of iron for magnetic nanoparticles, or as grams of gold for plasmonic nanoparticles. This comparison was conducted on 20-nm iron oxide nanocubes and

25-nm gold nanostars (similar nanoparticle size). As we can see on the thermal images (Fig. 3A), the nanostar-mediated plasmonic PTT is the only one to be efficient at low concentrations (0.05 $g_{Au\ or\ Fe}$/L). In contrast, at high concentrations (5 $g_{Au\ or\ Fe}$/L), the difference between MHT and magnetic PTT is less pronounced and the difference between magnetic PTT and plasmonic PTT is negligible. The averaged calculated SAR (Fig. 3C) confirms that for MHT, the SAR is concentration independent, of 400 W/g_{Fe} (at 18 mT and 470 kHz). For magnetic and plasmonic PTT, at low concentrations (0.05 g_{Au}/L), the SAR is impressively high (3 kW/g_{Fe} and 25 kW/g_{Au}, at 1 W/cm^2, for magnetic and gold nanoparticles, respectively). By contrast, at 5 g_{Fe}/L, the SAR obtained for both magnetic and plasmonic PTT at 1 W/cm^2 is comparable with the one obtained in MHT (in the 500 W/g_{metal} range). As expected from the reasoning above, together with the high extinction coefficient of gold nanoparticles (Table S1), plasmonic PTT is more impaired by higher particle concentrations than magnetic PTT. As a result, at low (0.05 g/L) doses, plasmonic SAR is 8-fold higher than magnetic SAR; at medium (0.5 g/L) doses, the difference is only 3-fold; and at high doses, plasmonic and magnetic SARs are of the same order. The theoretical SAR_{theor} are also presented in Fig. 3C, superimposed to the experimental values, and in very good agreement. Note finally that the calculated photothermal conversion efficiency of gold nanostars η = (38 ± 3) % is logically higher than the one of iron oxide nanocubes η = (29 ± 2) %.

The intermediate conclusion related to the role of nanoparticles concentration is that at low nanoparticle doses, we can only rely on PTT (magnetic or plasmonic, and only plasmonic at very low doses). In contrast, at high concentrations, MHT takes over its advantage, all the more so because there are no limitations in terms of treatment depth. In addition, at high nanoparticle concentrations, magnetic PTT is as advantageous as plasmonic PTT, placing iron oxide nanoparticles at the forefront of thermal therapies, which require local (*e.g*. intratumoral) injections. Conversely, at low concentrations, as for instance the ones obtained after systemic administration, plasmonic PTT appears as the only approach that might be therapeutically viable.

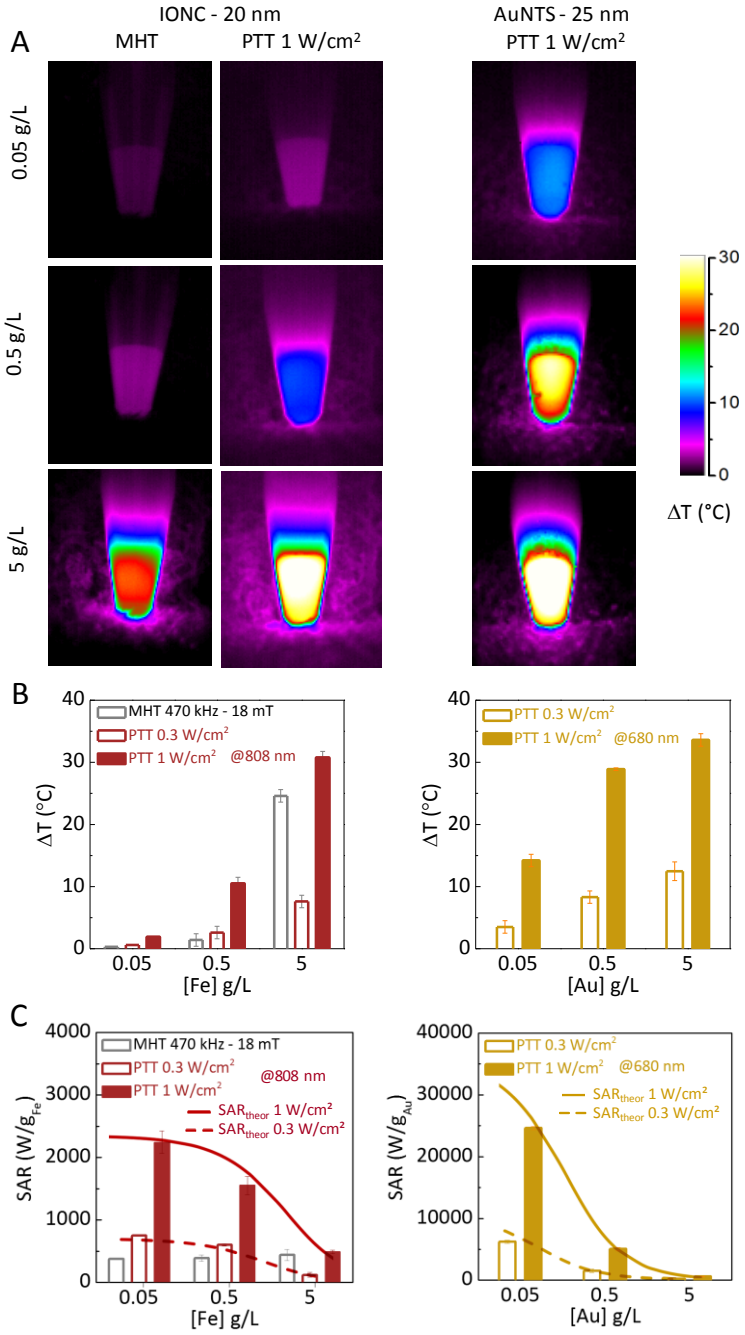

Fig. 3. Heating effect of iron oxide nanocubes and gold nanostars as a function of concentration. A. Infrared thermal images of (left) aqueous dispersions of iron oxide nanocubes (IONC - 20 nm,) after 1 min of MHT (470 kHz – 18mT) and PTT (1 W/cm^2) and (right) of gold nanostars dispersions (AuNST – 25 nm) subjected to 1 min of PTT (1 W/cm^2) at different concentrations of Fe and Au (0.05, 0.5 and 5 g/L). Note that the selected concentrations contain similar masses of Fe and Au. **B,C.** Temperature elevations (B) and heating capacities SAR (C) of IONC - 20 nm and AuNST – 25 nm subjected to MHT and PTT at different conditions as a function of iron or gold concentration. On the SAR plots, the theoretical SAR_{theor}, calculated according to equation (1), are superimposed on each graph.

3. The effect of intracellular processing

As nanoparticles are intended for a potential therapeutic application, it is essential to evaluate the heating behavior in the (cancerous) cell with its intracellular environment. First of all and regardless of their type, the nanoparticles enter via endocytosis and concentrate within endosomes (Figs. 4A and 5A, Figures S3 and S4). This intracellular processing impacts the physical properties of nanoparticles, for instance magnetic nanoparticles in cell conditions exhibit lower initial susceptibility and hysteresis loop opening for most nanoparticles (Figure S5). Cells containing iron oxides or gold were dispersed to reach an equal overall concentration of 25 mM in iron for magnetic nanoparticles (Fig. 4) or 0.75 mM in gold for plasmonic nanoparticles (Fig. 5). Note that these cellular samples concentrations were identical to those previously assessed in aqueous suspensions. Fig. 4B illustrates the effect of cellular internalization on the heating production through MHT. Irrespective of the nanoparticle type, heating was found to be drastically reduced. The most striking effects were observed in the case of IONFs, with a 85% heating loss, or for CFNPs, with as 90% heating loss. Such an effect was previously reported, and generally attributed to the inhibition of Brownian relaxation.[40-42] This decrease upon confinement of nanoparticles in the endosomes, is even more pronounced for nanoparticles for which the anisotropy or the inter-particle exchange interactions favor Brownian relaxation. Nevertheless, a marked (40%) decrease also applies to rock-like IONPs, for which the heating involves mainly Néel relaxation, suggesting that strong inter-particle interactions can also be harmful to Néel-relaxing nanoparticles. Besides, even if the decrease of heating in the cellular environment is reduced for the latter nanoparticles, they initially have a lower SAR. As a consequence, for nanoparticles localized within cells, the SAR never exceeds 60 W/g (for IONC), and falls below 20 W/g for IONP, CFNP, and IONF.

The fact that, to date, no nanoparticles were yet described to enable sufficient heating within the cellular environment for MHT, has raised interest on therapeutic alternatives, which allow overcoming the intracellular-heating issue. One strategy consists of applying magnetic nanoparticles with aminosilane coating, which prevents nanoparticles from entering the cells (this strategy was used by MagForce AG, The Nanomedicine Company),[43] whereas a second alternative comprises functionalization of magnetic nanoparticles with membrane ligands, which specifically target membrane receptors of a given cell type, with an induced cytotoxic response which does not involve global heating on the cellular level.[19, 44]

Conversely, when we analyze the photothermal heating performance of magnetic nanoparticles (Figure 4C), the situation is different; and even reversed. For all tested nanoparticle groups, heating is maintained, and is even greater once the cells have internalized (confined) the particles. In the particular case of IONCs, we can now juxtapose the PTT-derived intracellular SAR of 1200 W/g_{Fe} (obtained with a laser density of 1 W/cm^2) with the modest 60 W/g_{Fe}, obtained with MHT (470 kHz, 18mT). We thus obtain a counterintuitive result: IONCs, considered among the best MHT agents,[45] have now manifested as 20 times more efficient mediators of PTT.

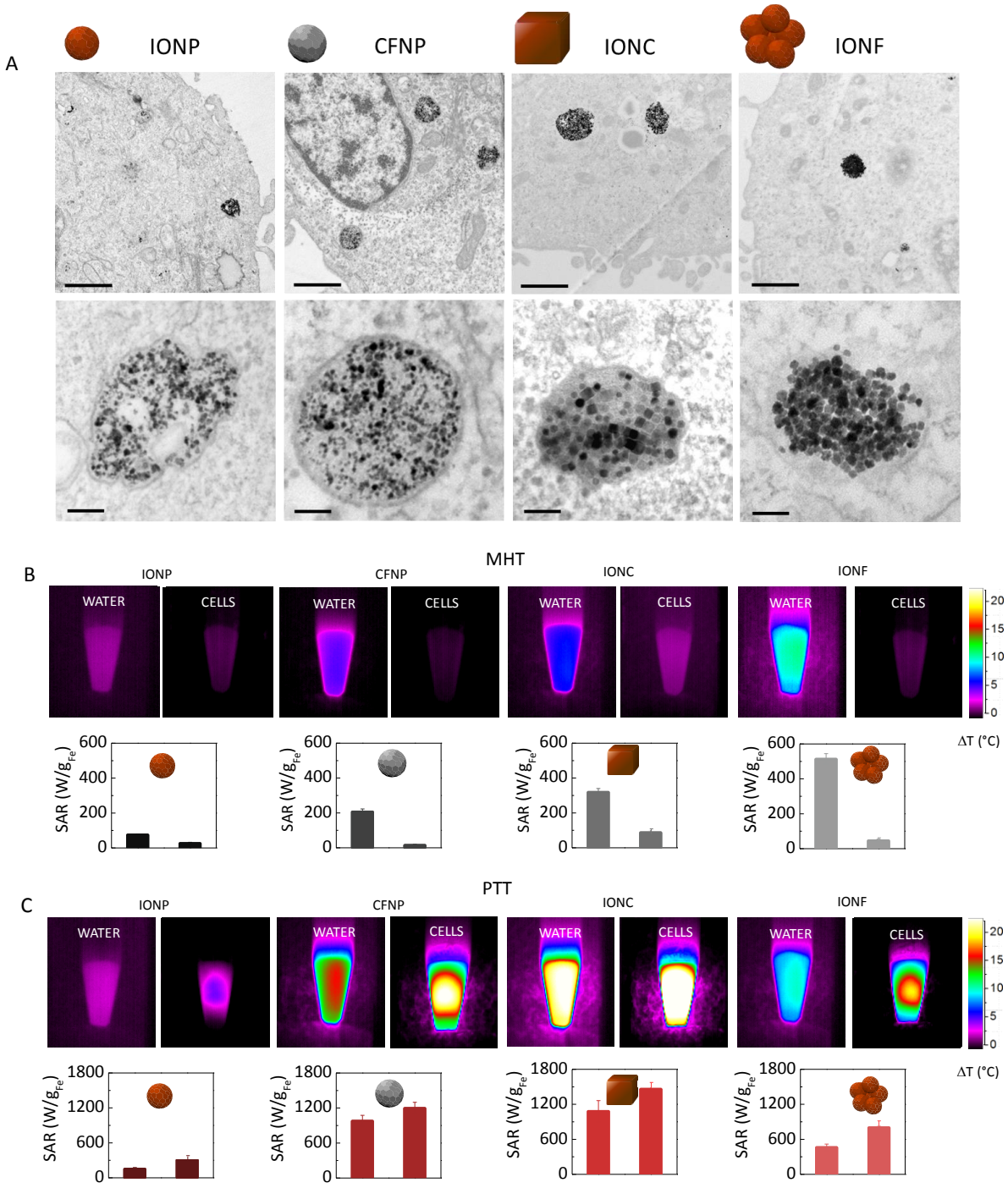

Fig. 4. Heating of magnetic nanomaterials inside cancer cells (*in vitro*). A. TEM micrographs of magnetic nanomaterials confined within endosomes after incubation in cancer (PC-3) cells. Scale bars: 1 μm (top views); 100 nm (bottom zoomed views). **B, C**. Panels comparing infrared images of aqueous suspensions of cells loaded with magnetic nanoparticles, (**B**) after 1 min of applying MHT (470 kHz -18 mT), and (**C**) after 1 min PTT (808 nm, 1 W/cm^2). All samples contain the same iron concentration ([Fe] = 25 mM, 1.4 g/L). For both, the average heating efficiencies are also shown in terms of SAR (W/g$_{Fe}$).

Regarding more conventional (plasmonic) PTT agents (Figure 5), the effects of cell internalization (Figure 5A) are mostly beneficial, due to plasmonic coupling in endosomes.[21, 46-50] When 25-nm gold nanostars (AuNST-1) or 85-nm gold nanostars (AuNST-2) are excited at wavelengths resonant with their plasmon band (680 nm, or 808 nm, respectively), heating within cells is comparable to that in aqueous dispersion (Figure 5B). However, while small nanostars (AuNST-1), excited with the wavelength of 808 nm, do not heat considerably in suspension, because the excitation wavelength does not correspond to their plasmon band, cell-internalized AuNST-1 do respond to the excitation at 808 nm light. And they do it as efficiently as their 85-nm counterparts, which actually have the plasmon band centered at 800 nm. This result is a direct consequence of plasmon red-shift and band broadening, due to plasmon coupling between neighboring nanostars. The consequences of cell internalization can thus be favorable for plasmonic nanoparticles (e.g. 300% heating increase for 25-nm AuNSTs at the excitation wavelength of 808 nm). This phenomenon is compelling for *in vivo* applications, because smaller (25-nm) nanostars might have a more favorable bio-distribution than larger (85-nm) nanostars, and the laser wavelength to be applied (about 800 nm), would be absorbed by bodily components to a smaller degree.

When a direct comparison is made between the heating of magnetic and plasmonic nanoparticles after cellular processing, we can state that plasmonic nanostars are much more efficient heating agents in PTT (7500 W/g_{Au}, 1 W/cm^2) than iron oxide nanocubes for MHT (60 W/g_{Fe}, 470 kHz-18 mT). Nevertheless, when magnetic nanocubes are used in PTT, their output (1200 W/g_{Fe}, 1 W/cm^2) is getting closer to that of gold nanostars.

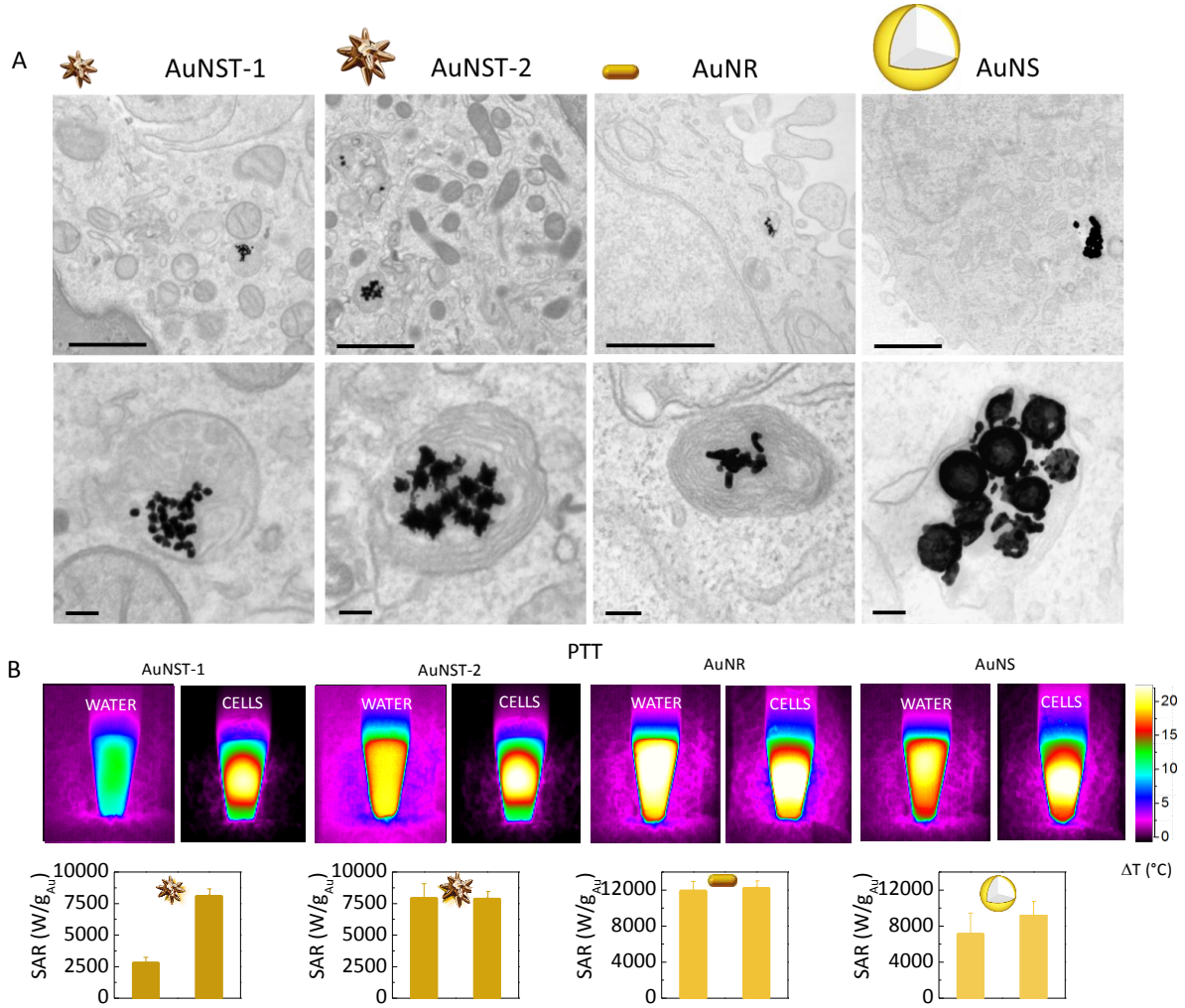

Fig. 5. Heating of gold nanoparticles inside cells (*in vitro*). A. TEM micrographs of plasmonic nanomaterials after incubation in PC-3 cancer cells (scale bar 200 nm). Note that for nanoshells, cutting into 70-nm sections is probably responsible of the small pieces detected when a 200-nm nanoshell is cut at the top of the sphere. **B.** Infrared images of gold nanoparticles dispersed in water of loaded within cells after 1 min of PTT (808 nm, 1 W/cm^2). All samples contain the same gold concentration ([Au] = 0.75 mM, 0.1 g/L)). The comparison between heating efficiencies in both media are represented in dedicated graphs (SAR (W/g$_{Au}$)).

Taken together, these measures indicate that MHT is impaired after particles are internalized by cells, and that even the most efficient magnetic nano-heaters, such as iron oxide nanocubes or nanoflowers, loose their heating power (e.g. up to 95%, as shown in nanoflowers). Conversely, in plasmonic PTT, the heating efficacy can be increased, as evidenced for 25-nm gold nanostars. And, in between the two extremes, in magnetic PTT, the internalization did not negatively affect the heating, but it rather slightly increased the heating within the intracellular environment.

4. Heating efficacy *in vivo*

Finally, what can we possibly expect to happen within the tumor, which is the final target of thermal anticancer treatments? As we mentioned above, moderate hyperthermia can sensitize the tumors to chemotherapeutics and radiation and, as shown in animal models, can slow down tumor growth[16, 24, 51-55] and stimulate the immune system,[56, 57] but does not lead to complete tumor ablation (or total tumor regression). Tumor ablation is generally observed only when higher temperatures (43 °C and above) are obtained within the tumor core.[21, 58]

In the comparison between MHT and PTT *in vivo,* we focused on the 20-nm magnetic iron oxide nanocubes and 25-nm plasmonic gold nanostars. The intratumoral heat increase was measured 1 h after the intratumoral injection of increasing concentrations (100 µL at 0.05, 0.5, 5 g/L; which corresponds to the following administered doses of about 0.25, 2.5 and 25 mg/kg body weight) of either iron oxide or gold nanoparticles.

Remarkable and reassuring, at injection day, intratumoral heating responses (Fig. 6) were comparable to those observed in aqueous suspensions of the same nanoparticles (Fig. 3), and allowed us to obtain the following results: (i) in the MHT setting, a relevant temperature increase occurs only at the highest particle concentration, and the intratumoral temperature increase is proportional to the injected dose, falls below 1°C for the 0.5 g/L dose and equals 7.5°C for the 5 g/L dose; (ii) PTT is efficient at low particles concentration, and increasing particle concentrations are not particularly beneficial, especially for plasmonic PTT. Typically, if we increase the concentration by 100 times (from 0.05 to 5 g/L) we only get a 3-fold temperature increase for nanostars, and 4-fold increase for nanocubes. Nevertheless, at concentrations of 0.05 g/L, nanostars are most efficient, with a temperature increase of 10°C (at 1 W/cm² exposure), in the therapeutic range. For nanocubes, at such a low dose of 0.05 g/L, the temperature increase is only 5°C (at 1 W/cm²). At the higher dose of 5 g/L, both nanostars and nanocubes provide therapeutic heating of 10°C and 8°C, respectively, at a lower laser power of 0.3 W/cm².

For magnetic nanocubes, the dose was finally increased to 12.5 g/L, closer to amounts injected for MHT in pre-clinical trials. For MHT, as expected, the temperature increase is linear (18°C), competing with magnetic PTT at 1 W/cm² (22°C increase), and overpassing it at 0.3 W/cm² (9°C increase).

Note that 1 W/cm^2 laser power density should be considered the upper limit of PTT setting. Although not recommended, it is however commonly used in pre-clinical settings. Besides, laser power densities of 2, even 3 W/cm^2, are sometimes also reported, while they generate a considerable thermal response within the exposed tissue,[59] which is not specific to heating nanoparticles. In our setting, the non-specific heating, attributed to the laser power density of 1 W/cm^2 was of almost 5°C at 680 nm, 3°C at 808 nm. By contrast, a power of 0.3 W/cm² results in almost no non-specific heating (below 2°C at 680 nm, below 1°C at 808 nm). It thus appears that, to avoid thermal response to the laser, power densities as low as 0.3 W/cm^2 should be preferred. It is difficult to find general guidelines on the selection of laser power in pre-clinical studies. Only rare studies use 0.3 W/cm² as a safe limit.[60, 61] In this 0.3 W/cm² setting, magnetic and plasmonic PTT are then only applicable at the 5 g/L dose, for a temperature increase in the 10°C range.

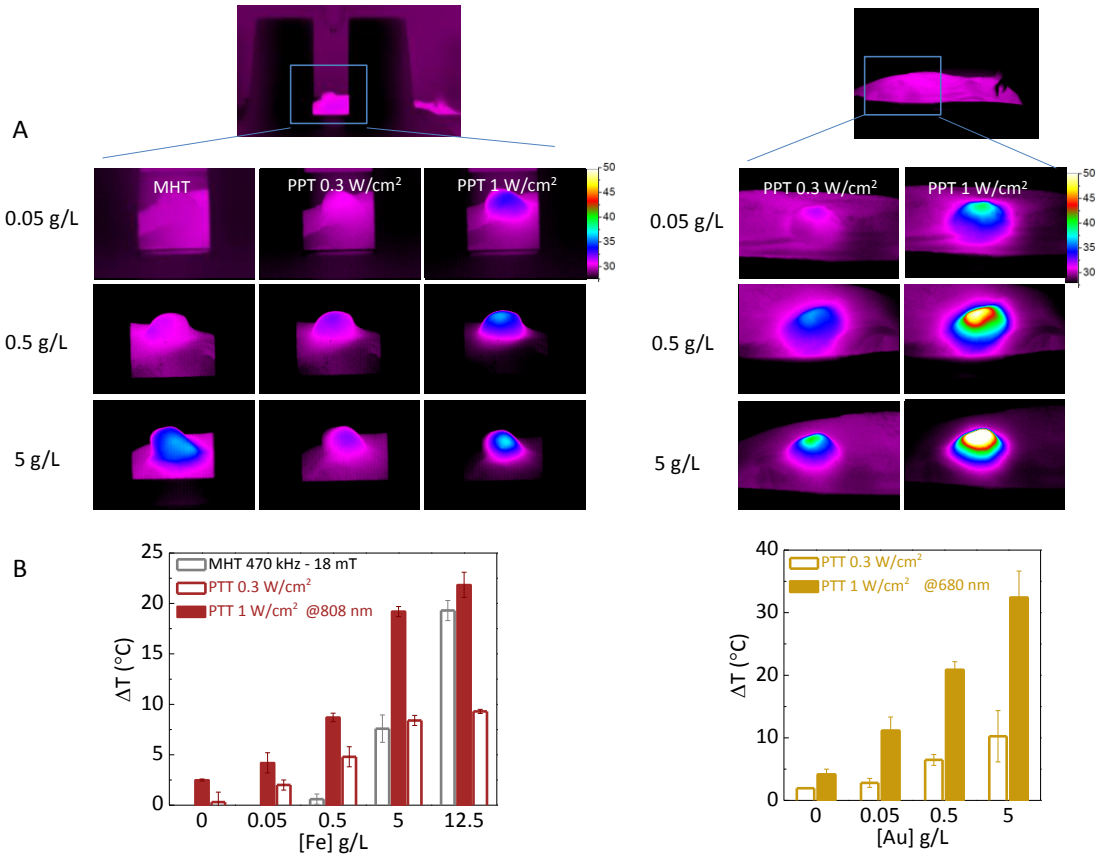

Fig. 6. Intratumoral heating of iron oxide nanocubes and gold nanostars (*in vivo*). **A**. Infrared thermal images after intratumoral injection of (left) 20-nm IONC suspension in mice followed by MHT (470 KHz, 18 mT, 5 min) or PTT (808-nm, 0.3 and 1 W/cm^2, 5 and 1 min, respectively) and (right) 25-nm AuNST in mice after PTT (808-nm, 0.3 and 1 W/cm^2, 5 and 1 min, respectively). These thermal measurements were taken at

day 0 after injection. **B**. Graphs representing the average temperature increase as a function of iron or gold concentration, after MHT or PTT at 0.3 or 1 W/cm² laser exposure.

Finally, we address the effect of cell internalization *in vivo*, and compare the heating effects at the day of injection (day 0) and 3 days after injection (day 3). The comparison was made, in this case, at concentrations of 12.5 g/L (62.5 mg/kg) for nanocubes and 0.15 g/L (0.75 mg/kg) for the 25-nm and 85-nm nanostars (Figure 7). These conditions were chosen to obtain a temperature increase of 10-20°C. Nanocubes submitted to MHT provided a temperature increase of 18°C at day 0. After laser exposure at 808 nm (1 W/cm², non-specific heating of 3°C), we obtained a temperature increase of 22°C for nanocubes and 8°C or 14 °C for 25-nm and 85-nm nanostars, respectively.
At day 3, the heating efficiency of MHT drops below 10°C increase, while magnetic PTT is slightly more efficient than at day 0 (25°C increase). For plasmonic PTT, the heating efficiencies of 25-nm AuNST-1 and 85-nm AuNST-2 after laser excitation at 680 nm or 808 nm, respectively, decrease at day 3. This decrease most likely correlates with nanostars permeation throughout the tumoral interstitial space and gradual clearance from the tumor. The spreading of the particles throughout the tumor matrix has been reported in previous studies and correlates with particle size,[62] with gold nanoparticles below 100 nm exhibiting a more pronounced spreading throughout the tumor. At low concentration ranges, concentration variations impact the heating to a greater extent and the permeation of nanoparticles (and the concomitant local decrease in nanostars concentration) result in a decrease of the heating. As the administered dose of nanostars was relatively low, the heating of the tumor at day 3 diminished on the account of the fraction of nanostars that was cleared from the tumor. On the other hand, nanocubes were administered in a 10-fold higher dose, where concentration variations have a lower effect on the heating outcome, thus even if a fraction of nanocubes are cleared from the tumor, the amount was too low in proportion to the administered dose, and did not substantially affect the PTT outcome at day 3.
That being said, in addition to particle spreading and gradual clearance from the tumor, the internalization of particles by adjacent cells also comes into play. It first explains the decrease in MHT efficiency from day 0 to day 3. Fig. 7C (together with Figures S6 and S7) provides the intratumoral localization of nanocubes at day 0 (mainly extracellular) and at day 3 (partly internalized within tumor cells). Logically, the significant cell internalization at day 3 translated into a decrease in the heating

performance of nanocubes for MHT. Interestingly, as observed *in vitro* in cells, the magnetic PTT is not affected by cell internalization *in vivo*, and even favored by the intracellular localization of nanocubes. Concerning plasmonic nanostars, electron microscopy (Fig. 7F, and Figures S8 and S9) shows that nanostars were almost all individual, dispersed in the extracellular matrix at day 0, while they were all internalized within cells at day 3. As a result, and as observed *in vitro* in cells for small 25 nm nanostars AuNST-1, the heating of the tumors at day 0 and day 3 remained comparable after irradiation at 808 nm, while it decreased at 680 nm. In this case, the remaining nanostars at day 3, internalized by the cells, compensated the total heating outcome by increasing their heating output. 25 nm AuNST-1 are then as efficient as 85 nm AuNST-2 at 808 nm.

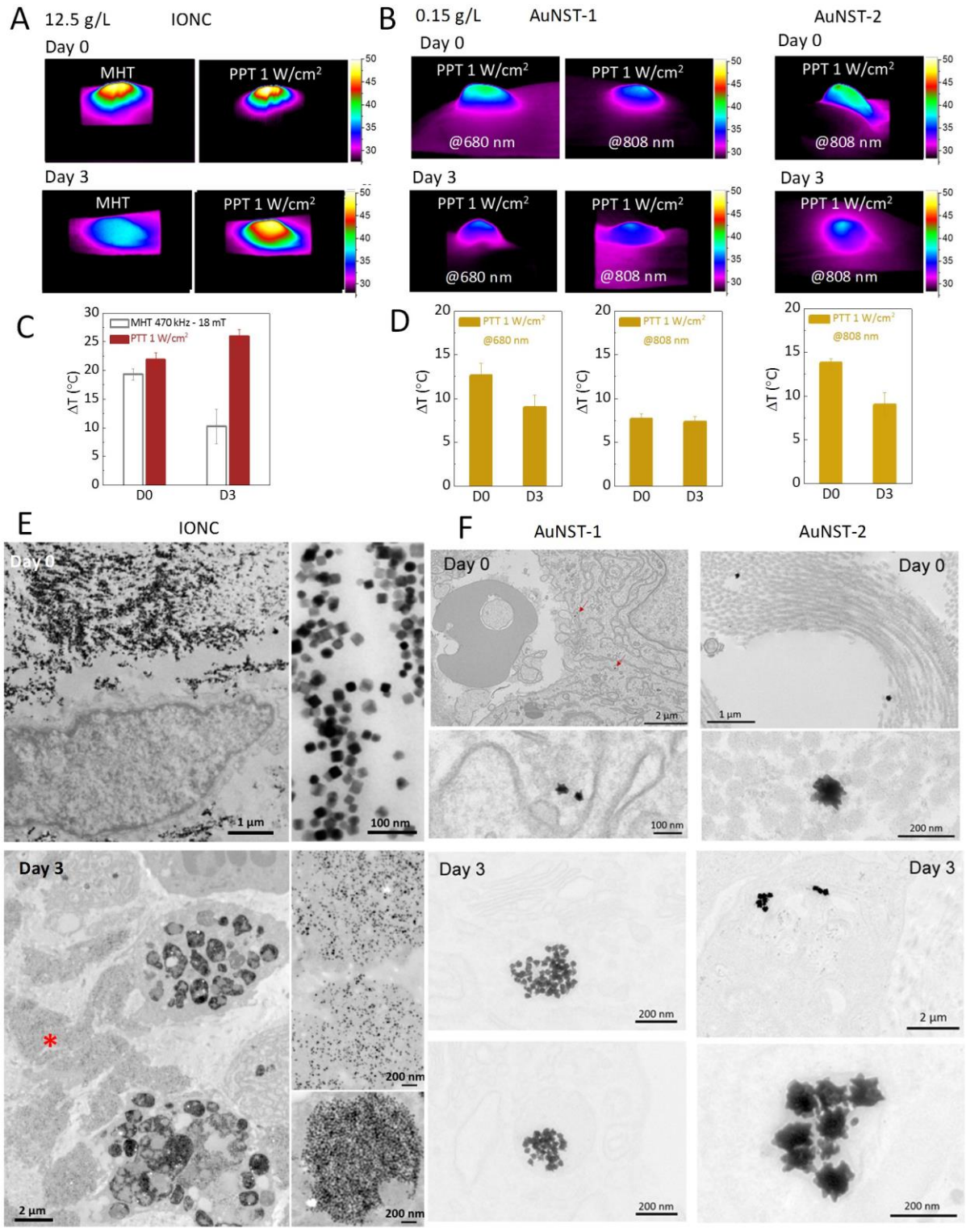

Fig. 7. Evolution of nanomaterials heating within tumors as function of time (*in vivo*). Infrared thermal images and temperature elevations at day 0 and day 3 for (**A**) the 20-nm IONC at [Fe] = 12.5 g/L (250 mM) after MHT and PTT treatments and for (**B**) the 25-nm AuNST at [Au] = 0.15 g/L (0.75 mM) subjected to PTT. **C**. TEM micrographs of IONC and AuNST in tumors at day 0 and day 3.

In summary, in order to attain therapeutically relevant temperature increase *in vivo*, we require smaller doses of gold nanostars in comparison to iron oxide nanocubes. Alternatively, for a temperature increase of 15-20°C, we need either 12.5 g/L (62.5 mg/kg) of nanocubes for MHT (at 470 kHz and 18 mT) or 0.5 g/L (2.5 mg/kg) of nanostars for plasmonic PTT at a laser power density of 1 W/cm^2. Nevertheless if the laser power density has to be decreased due to the laser-induced non-specific heating, and a laser dose of 0.3 W/cm^2 has to be applied, only a 10°C temperature increase can be obtained with gold nanostars. Such temperatures are not sufficient for complete tumor ablation, but might slow down the tumor growth or be used as adjuvant therapy to other non-thermal treatments of cancer. As for the magnetic PTT at 0.3 W/cm^2 we are also limited to a temperature increase of about 10°C, which is obtained either with 5 or 12.5 g/L (25-62.5 mg/kg). As saturation is already reached at 5 g/L, increasing particle dose does not lead to an increased heating of the tumor.

Consequently, if we compare a "safe" plasmonic or magnetic PTT at 0.3 W/cm^2, which, due to saturation effects can only allow a 10°C increase, MHT has the advantage of increasing the temperature to a much greater extent (e.g. 20°C). Thus, the obtained results indicate that if high temperature increments (>10°C) are required *in vivo* and non-specific heating has to be avoided, MHT remains the only option.

CONCLUSIONS

Magnetic hyperthermia (MHT) and photothermal therapy (PTT) are two promising emergent treatments against cancer. Until very recently, the development of these two modalities advanced along two parallel paths, with magnetic (iron oxide) nanoparticles leading the field of MHT and plasmonic (gold) nanoparticles "striking the gold" in the field of PTT. Yet, magnetic materials may also generate heat upon exposure to light. In this nanoparticles-based thermal therapy context, it appeared timely to provide a comprehensive comparison of the outcome of magnetic versus plasmonic heating. In a head-to-head basis, we confronted different magnetic nanoparticles (iron oxides, cobalt ferrite, spheres, cubes, flowers) with different plasmonic (gold, stars, rods, shells) nanoparticles in aqueous, cellular, and tumoral environment.

For comparison in water, we have chosen to compare relevant concentrations of apposite materials (25 mM_{Fe} or 0.75 mM_{Au}) and the heating capacity (expressed as SAR in W/g) was substantially higher for plasmonic nanoparticles (almost 10 000

W/g_{Au}, 1 W/cm^2) in comparison with magnetic nanoparticles (max 400 W/g_{Fe}). Nevertheless, this confrontation should be taken with caution. While SAR is an absolute indicator, concentration-independent in case of MHT, it decreases with the nanoparticles concentration for PTT. We thus compared the SARs at equivalent masses (g/L). While at 0.05 g/L of Fe or Au, the SARs of plasmonic nanoparticles is 100-times higher than the one of the best (nanocubes and nanoflowers) magnetic nanoparticles for MHT, at 5 g/L, the SARs are within the same orders of magnitude (400 and 800 W/g for MHT and plasmonic PTT, respectively). Besides, PTT with magnetic nanoparticles can compete with plasmonic heating, with a SAR of about 3000 and 600 W/g_{Fe} at 0.05 and 5 g_{Fe}/L (1 W/cm^2), respectively. Another key parameter that should be taken into consideration is the effect of cell internalization. The latter has a harmful impact on MHT, while it is beneficial for PTT applications in the near infrared, and the influence of concentration and internalization (confinement) is remarkable *in vivo*.

As for what concerns the excitation source, in order to obtain a therapeutic temperature increase (of about 10°C) at a physiologically inert laser power density (of 0.3 W/cm^2), plasmonic and magnetic nanoparticles should be used at relatively high doses (0.5 g/L or 5 g/L, equivalent to 2.5 or 25 mg/kg doses, for plasmonic and magnetic nanoparticles, respectively). The magnetically heated iron oxide nanoparticles can lead to an even higher temperature increase (typically of about 20°C at the highest iron concentration used in this study, which is 12.5 g_{Fe}/L). Such temperatures can, in principle and in pre-clinical practice, be obtained with gold nanostars at 0.5 g_{Au}/L or magnetite nanocubes at 5 g_{Fe}/L, and a laser power density of 1 W/cm^2, but as mentioned above, this laser power density is less appropriate in clinics. In addition, increasing the concentration of gold nanoparticles at low laser power densities will not lead to a temperature increase above 10°C, which makes MHT the modality of choice for a temperature increase of 20°C, with no collateral unspecific heating. Yet again, this setting will require a very high dose of iron oxide nanoparticles (12.5 g_{Fe}/L). A dose that slowly but surely undergoes gradual internalization within cells and consequently diminishes the efficacy of MHT in the days following the injection. The effects of cell internalization have a smaller impact when large quantities of magnetic nanoparticles are used for MHT (because the fraction of internalized particles versus the extracellular ones remains small), but the heating still decreases in the days following the particles administration.

Overall, these findings enable us to conclude that there are two therapeutic applications of the two modalities: one pertaining to low doses, where PTT is effective, but the temperature increase can be limited to 10°C or requires the laser power density of 1 W/cm^2, or, alternatively, a MHT application, where a high dose of magnetic nanoparticles is required.

MATERIALS and METHODS

1. Synthesis of magnetic nanomaterials

1.1 Iron oxide and cobalt ferrite nanoparticles: Iron oxide (maghemite) nanoparticles were synthesized by alkaline co-precipitation followed by a forced oxydation by iron nitrate treatment. Cobalt ferrite nanoparticles were obtained by precipitation of a stoechiometric mixture of Co(II) and Iron (III) hydroxyde followed by heating at 100°C for 1 hour. After nitric acid treatment, magnetic nanoparticles were capped with citrate ions to ensure their stability in aqueous suspension by electrostatic repulsion (negative surface charges).

1.2. Iron oxide nanocubes: To obtain nanocubes of magnetite 20 nm in edge length, first, 1 mmol of iron(III) acetylacetonate and 4 mmol of decanoic acid were mixed in 25 mL of dibenzyl ether (according to the protocol detailed by Guardia et al.[45]). The temperature of the solution was increased to 220°C using a progressive heating of 5°C/min and then kept at this temperature for 2.5 h. Finally, the solution was heated to reflux temperature (at a rate of 10°C/ min) and reacted for 1 h. The cubes were rinsed three times and dispersed in 15 mL of chloroform and then mixed with a PEG-gallol solution (20 mL, 0.05 M in $CHCl_3$) together with triethylamine (2 mL); finally, the mixture was transferred to water.

1.3. Iron oxide nanoflowers: Iron oxide (maghemite) nanofowers were prepared via the polyol process.[23] A mixture of $FeCl_3$ and 2 mmol of $FeCl_2$ (in a liquid mixture of N-methyldiethanolamine and diethylene glycol) was stirred for 1 h. A sodium hydroxide solution (in polyols) was added to the solution of iron chloride, and the resulting mixture was stirred for additional 3 h. Then, the temperature was increased to 220°C and the mixture kept reacting for 12 h. The precipitated were separated magnetically and washed with a mixture of ethanol and ethyl acetate. Then, an aqueous solution of iron(III) nitrate was added to the nanoparticles. The resulting mixture was heated to 80°C for 45 min to achieve a complete oxidation of the nanoparticles. After another

treatment with 10% nitric acid, the particles were rinsed twice with acetone and diethyl ether and finally dispersed in water.

2. Synthesis of metallic nanomaterials

2.1 Gold nanostars: Gold nanostars were prepared by following the protocol by Kumar et al.[63] Briefly, an aqueous solution of $HAuCl_4$ (0.041 mL, 100 mM) was mixed with a solution of PVP (15 mL, 10 mM) in DMF. The mixture was stirred until complete disappearance of the Au^{+3} CTTS band at 325 nm, followed by rapid addition of gold seeds in ethanol under vigorous stirring. To obtain nanostars with 25 and 85 nm of diameter, the volume of seeds was found to be 0.292 mL and 0.159 mL, respectively. The color of the solution changes from colorless to blue within 40 minutes, indicating the formation of gold nanostars. The samples were centrifuged three times and redispersed in water.

2.2 Gold nanorods: Gold nanorods, with an approximate aspect ratio of 3.5 (length 41 nm, width 11 nm) were prepared following a well-established seeded growth approach described previously,[27] with minor modification. Briefly, spherical gold seed particles were synthesized by mixing 1 mL of 5×10^{-4} M $HAuCl_4$, 1 mL of 0.2 M CTAB and 0.12 mL of ice cold 0.01 M $NaBH_4$. The suspension was vigorously mixed for 2 minutes at 1800 rpm on an orbital shaker (Heidolph MultiReax) and then for 1 hour at 1000 rpm. Thereafter, 0.12 mL of the fresh prepared gold seeds was added to a solution containing 50 mL of 0.2 CTAB, 2.5 mL of $AgNO_3$ 4×10^{-3} M, 50 mL of $HAuCl^4$ 10^{-3} M and 0.7 mL of ascorbic acid 0.078 M. The resulting mixture reacted for 30 minutes at 1200 rpm. The described steps were performed at room temperature. The gold nanorods were separated by centrifugation (10 minutes at 14000 rpm) and resuspended in ultrapure water.

2.3 Gold nanoshells: Au silica-nanoshell suspensions were purchased from Nanospectra Biosciences, Inc. (Houston, USA). The nanoshells consist of a 150 nm silica-core diameter, surrounded by an ultra-thin 8 nm thick gold shell, conjugated with polyethylene glycol (PEG).

3. Cell culture and internalization assays

For the *in vitro* measurements, human prostate cancer cells (PC-3 cells) were cultured in Dulbecco's modified Eagle's medium (DMEM) supplemented with 5% fetal bovine serum (FBS) and 1% penicillin, and maintained at 37°C with 5% CO2 until confluence. The cells were co-incubated for 2 h with the different magnetic colloids, at the following concentrations within the extracellular medium: [Fe] = 2 mM for iron oxide

nanoparticles and for cobalt ferrite nanoparticles, [Fe] = 0.2 mM for iron oxide nanocubes and [Fe] = 0.6 mM for iron oxide nanoflowers. The magnetic particles were dispersed in serum-free RPMI-1640 medium supplemented with 5 mM sodium citrate. At the end of the incubation, the medium was removed and the cells were rinsed three times with culture medium, and further placed at 37°C for an additional 2 h chase period.

For the metallic nanoparticles, the cells were incubated at [Au] = 0.02 mM for 12 h in RPMI medium (for 25-nm and 85-nm nanostars) and in DMEM medium supplemented with 5% fetal bovine serum (FBS) and 1% penicillin.

Particle-loaded cells were detached by means of trypsin-EDTA solution and resuspended in PBS in order to obtain 150 µL (approximately 20 million cells) and transferred into a 0.5 mL-Eppendorf tube. The cell fraction that was intended for TEM analysis was fixed with glutaraldehyde (2%) in 0.1 M sodium cacodylate buffer (7.4 pH) at 4 °C for 60 min, and stained with 1% osmium tetroxide in cacodylate buffer. The cells were subsequently dehydrated with graded solutions of ethanol, impregnated with hexa-methyl-phosphor-amide, and embedded in EPON resin supplemented with 3% benzyl-dimethyl-amine.

4. Elemental analysis

The concentrations of iron and gold in aqueous dispersions and in cells were measured by elemental analysis using an ICP-AES spectrometer (iCAP 6500, Thermo). The samples were digested in a HNO_3 and HCl solution (10 mL) using appropriate iron and gold standards. The iron load per cell was additionally determined by single-cell magnetophoresis.

5. Transmission electron microscopy

Cells or $1mm^3$ tumor tissue pieces were fixed with glutaraldehyde (2%) in 0.1 M sodium cacodylate buffer (7.4 pH) at 4 °C for 60 min, and stained with 1% osmium tetroxide 1.5% and potassium cyanoferrate in cacodylate buffer. The cells/tissues were subsequently dehydrated with graded solutions of ethanol, impregnated with hexa-methyl-phosphor-amide, and embedded in EPON resin supplemented with 3% benzyl-dimethyl-amine.

TEM micrographs of aqueous dispersions were obtained with a FEI-Philips TECNAI 12 transmission electron microscope. Thin sections (70 nm) of cells and tumors were observed with a Zeiss EM902 electron microscope operating at 80 keV (MIMA2 - plateau de MET - unité 1196 GPL - Jouy-en-Josas, France).

6. Thermal measurements

Thermal measurements of nanomaterials in aqueous dispersion and within cells were performed in Eppendorf tubes (0.5 mL) containing 150 µL of sample. Concentrations were adjusted to [Fe] = 25 mM (1.2 g/L) for magnetic nanomaterials and [Au] = 0.75 mM (0.1 g/L) for metallic nanomaterials, which are in the range of standard element content to induce an elevation of temperature of 10-20°C.

An alternating magnetic generator device (DM3, NanoScale Biomagnetics) with a frequency ranging of 470 kHz and 18 mT of amplitude was used to induce MHT. The sample was placed between two magnetic coils.

For PTT, each sample was illuminated with visible and NIR lasers (680 or 808 nm) coupled to an optic fiber (Laser Components S.A.S (France)) at 1 and 0.3 W cm^{-2} and imaged with an infrared camera (FLIR SC7000) in order to measure the temperature increase.

The temperature elevation was measured as a function of time (dT /dt) at the initial linear slope (t = 30 s) in order to evaluate the heating effect in terms of SAR, power dissipation per unit mass of element, iron or gold, (W. g^{-1}). SAR was calculated using the following formula:

$$SAR = \sum_i \frac{m_i.C_i}{m_{Fe\ or\ Au}} . \frac{dT}{dt}$$

where $m_{Fe/Au}$ is the total mass of iron or gold in the sample, m_i is the nanoparticle element mass and C_i to the specific heat capacity of the component i. Since the mass of the heating element and its heat capacity (C_{Fe} = 0.449 $J.g^{-1}.K^{-1}$, C_{Au} = 0.129 $J.g^{-1}.K^{-1}$) are significantly lower than those of water or cell solution (C_w = 4.18 $J.g^{-1}.K^{-1}$, C_{cell} = 4.125 $J.g^{-1}.K^{-1}$), the initial equation can be written as:

$$SAR = \frac{m_w.C_w}{m_{Fe\ or\ Au}} . \frac{dT}{dt}$$

7. UV-Vis-NIR spectroscopy

Optical spectra were obtained using 50 scan Cary Spectrometer (Varian) in the 300–1100 nm spectral range.

8. Magnetic properties

Nanoparticle or cell suspensions (around 20 mg) were introduced in sample holding capsules for Vibrating Sample Magnetometer analysis (VSM, Quantum Design, Inc.).

Field-dependent magnetization curves were measured at 310 K as a function of the external field up to 3 T.

9. *In vivo* studies

In vivo experiments were performed in agreement with guidelines on animal care and use of Animalerie Buffon (Institute Jacques Monod, Paris 7). Studies on tumor bearing mice were carried out in 6 week old male immunodeficient athymic nude NMRI mice, with the mean weight of 30 g. The animals were provided by Janvier (France).

A total of 18 9-week-old female NMRI mice were used. The animals were allowed to acclimatize (Animalerie Buffon, Institute Jacques Monod, Paris 7 University) and were treated according to European standards of animal care and well-being. All animal experiments were approved by Buffon ethics committee (project reference CEB-07-2016).

Solid tumors were induced by subcutaneous injection of 1.5×10^6 PC-3 human epidermoid carcinoma cells in 100 µL of physiological saline in the left and right flanks. The animals were treated after two to three weeks, when the tumors reached approximately 125 mm^3. The animals were then, injected in one tumor with 100 µL of nanomaterials suspension at different concentrations: [Fe] = 0.05, 0.5, 5 and 12.5 g/L and [Au] = 0.05, 0.5 and 5 g/L, in order to compare the same mass element content. Three tumors were injected at each concentration.

The animals injected with magnetic materials were subjected to MHT (470 KHz, 18 mT, 5 min) and PTT (808-nm at 0.3 and 1 W/cm^2, 5 and 1 min, respectively) and those injected with metallic materials were subjected only to PTT (680 and 808-nm at 0.3 and 1 W/cm^2, 5 and 1 min, respectively. Some collateral tumors were used as controls (non-injected and non-treated). MHT and PTT experiments were conducted using the same instrument and set-up as in aqueous dispersion and *in vitro* studies.

During the measurements the animals were anesthetized with a ketamine/xylazine anesthesia. An infrared thermal camera (FLIR SC7000, FLIR Systems, Inc.) was used to monitor the surface temperature of the tumors.

REFERENCES

1. Huang, X. et al. *Lasers in medical science 23*, 217 (2008).
2. Hergt, R. et al. *Journal of Physics: Condensed Matter 18*, S2919 (2006).
3. Abadeer, N.S. et al. *The Journal of Physical Chemistry C 120*, 4691-4716 (2016).
4. Elzoghby, A.O. et al. *Journal of Controlled Release 243*, 303-322 (2016).
5. Hergt, R. et al. *Journal of Magnetism and Magnetic Materials 311*, 187-192 (2007).
6. Jain, P.K. et al. *J. Phys. Chem. B 110*, 7238-7248 (2006).
7. Rosensweig, R.E. *Journal of magnetism and magnetic materials 252*, 370-374 (2002).
8. Johannsen, M. et al. *International Journal of Hyperthermia 26*, 790-795 (2010).
9. García, M.A. *Journal of Physics D: Applied Physics 44*, 283001 (2011).
10. Bardhan, R. et al. *Accounts of chemical research 44*, 936-946 (2011).
11. Oei, A.L. et al. *Radiation Oncology 10*, 165 (2015).
12. Vaupel, P. et al. in Hyperthermia and the therapy of malignant tumors 71-109 (Springer, 1987).
13. Jain, R.K. *Cancer research 48*, 2641-2658 (1988).
14. Storm, F.K. et al. *Cancer research 39*, 2245-2251 (1979).
15. Kolosnjaj-Tabi, J. et al. *Pharmacological Research* (2017).
16. Kolosnjaj-Tabi, J. et al. *ACS nano 8*, 4268-4283 (2014).
17. Raeesi, V. et al. *Nanoscale 8*, 12524-12530 (2016).
18. Creixell, M. et al. *ACS nano 5*, 7124-7129 (2011).
19. Domenech, M. et al. *ACS nano 7*, 5091-5101 (2013).
20. Sanchez, C. et al. *ACS nano 8*, 1350-1363 (2014).
21. Espinosa, A. et al. *ACS nano 10*, 2436-2446 (2016).
22. Chu, M. et al. *Biomaterials 34*, 4078-4088 (2013).
23. Espinosa, A. et al. *Nanoscale 7*, 18872-18877 (2015).
24. Hirsch, L.R. et al. *Proceedings of the National Academy of Sciences 100*, 13549-13554 (2003).
25. Jacques, S.L. *Physics in medicine and biology 58*, R37 (2013).
26. Wang, X. et al. *RSC Advances 4*, 30375-30383 (2014).
27. Orendorff, C.J. et al. *The Journal of Physical Chemistry B 110*, 3990-3994 (2006).
28. Bucharskaya, A. et al. *International journal of molecular sciences 17*, 1295 (2016).
29. Jacques, S.L. *Surgical Clinics of North America 72*, 531-558 (1992).
30. Institute, A.N.S. American National Standard for safe use of lasers. (Laser Institute of America, 2007).
31. He, Y. et al. *Physical Review B 71*, 125411 (2005).
32. Fontijn, W. et al. *Journal of Applied Physics 85*, 5100-5105 (1999).
33. Tang, J. et al. *The Journal of Physical Chemistry B 107*, 7501-7506 (2003).
34. Plan Sangnier, A. et al. *Journal of Controlled Release 279*, 271-281 (2018).
35. Hu, Y. et al. *Chemical Society Reviews 47*, 1874-1900 (2018).
36. Blanco-Andujar, C. et al. in Iron Oxide Nanoparticles for Biomedical Applications 197-245 (Elsevier, 2018).
37. Yan, H. et al. *Advanced Functional Materials* (2018).
38. Roper, D.K. et al. *The Journal of Physical Chemistry C 111*, 3636-3641 (2007).
39. Tian, Q. et al. *Journal of the American Chemical Society 135*, 8571-8577 (2013).

40. Di Corato, R. et al. *Biomaterials 35*, 6400-6411 (2014).
41. Cabrera, D. et al. *ACS nano 12*, 2741-2752 (2018).
42. Soukup, D. et al. *ACS nano 9*, 231-240 (2015).
43. Jordan, A. et al. *Journal of neuro-oncology 78*, 7-14 (2006).
44. Clerc, P. et al. *Journal of Controlled Release 270*, 120-134 (2018).
45. Guardia, P. et al. *ACS nano 6*, 3080-3091 (2012).
46. Jain, P.K. et al. *Chemical Physics Letters 487*, 153-164 (2010).
47. Dykman, L.A. et al. *Chemical reviews 114*, 1258-1288 (2013).
48. Zhang, W. et al. *ACS applied materials & interfaces 5*, 9856-9865 (2013).
49. Comenge, J. et al. *ACS nano 10*, 7106-7116 (2016).
50. Espinosa, A. et al. *Advanced healthcare materials 5*, 1040-1048 (2016).
51. Di Corato, R. et al. *ACS nano 9*, 2904-2916 (2015).
52. Bae, K.H. et al. *ACS nano 6*, 5266-5273 (2012).
53. Ito, A. et al. *Cancer science 94*, 308-313 (2003).
54. Wust, P. et al. *International Journal of Hyperthermia 22*, 673-685 (2006).
55. Kossatz, S. et al. *Pharmaceutical research 31*, 3274-3288 (2014).
56. Multhoff, G. *International Journal of Hyperthermia 25*, 169-175 (2009).
57. Kobayashi, T. et al. *Nanomedicine 9*, 1715-1726 (2014).
58. O'Neal, D.P. et al. *Cancer letters 209*, 171-176 (2004).
59. Motamedi, M. et al. *Applied Optics 28*, 2230-2237 (1989).
60. Yang, Z. et al. *Theranostics 7*, 2177 (2017).
61. Jo, H. et al. *Journal of Materials Chemistry B 2*, 4862-4867 (2014).
62. Perrault, S.D. et al. *Nano letters 9*, 1909-1915 (2009).
63. Kumar, P.S. et al. *Nanotechnology 19*, 015606 (2007).